

Efficient second-harmonic emission via strong modal overlap in single-resonant lithium niobate nanocavity

Zhi Jiang,¹ Danyang Yao,^{1} Yu Gao,¹ Xu Ran,¹ Duomao Li,¹ Erqi Zhang,¹ Jianguo Wang,² Xuetao Gan,^{2*} Jinchuan Zhang,^{3*} Fengqi Liu,³ and Yue Hao¹*

¹State Key Laboratory of Wide-Bandgap Semiconductor Devices and Integrated Technology, School of Microelectronics, Faculty of Integrated Circuits, Xidian University, Xi'an, 710071, China;

²Key Laboratory of Light Field Manipulation and Information Acquisition, Ministry of Industry and Information Technology, and Shaanxi Key Laboratory of Optical Information Technology, School of Physical Science and Technology, Northwestern Polytechnical University, Xi'an, 710129, China;

³Laboratory of Solid-State Optoelectronics Information Technology, Institute of Semiconductors, Chinese Academy of Sciences, Beijing, 100083, China;

* dyyao@xidian.edu.cn; xuetaogan@nwpu.edu.cn; zhangjinchuan@semi.ac.cn;

ABSTRACT:

High-efficiency second-harmonic generation (SHG) in compact integrated photonic systems is crucial for advancing nonlinear optical technologies. However, achieving exceptional conversion efficiencies while maintaining stable performance remains a significant challenge. Here, we report a high-Q single-resonant photonic crystal nanobeam cavity (PCNBC) on a

polymer-loaded lithium niobate on insulator (LNOI) platform, which enables bright second-harmonic (SH) emission. Through synergistic optimization of modal confinement and spatial overlap in a y-cut LN architecture, our device achieves a normalized SHG conversion efficiency of 163%/W, outperforming previous LN-based photonic crystal cavities LN-based photonic crystal cavities by over three orders of magnitude. The visible SH emission at 768.77 nm exhibits a single-lobe radiation pattern with precise spectral alignment between fundamental (FH) and second-harmonic (SH) modes, a critical feature for integrated photonic circuits. Remarkably, the conversion efficiency remains stable under thermal variations up to 20°C, addressing a key limitation of multi-resonant systems. High-order cavity modes are directly visualized via CCD imaging, confirming strong spatial overlap. This work establishes a record SHG conversion efficiency for LN microcavities and provides a scalable, temperature-insensitive architecture for nonlinear light sources, with immediate applications in quantum optics and chip-scale interconnects.

KEYWORDS: nonlinear photonics, second-harmonic generation, photonic crystal nanobeam cavity, polymer-loaded lithium niobate, single-resonant cavity

■ INTRODUCTION

Integrated coherent light sources remain indispensable yet challenging components for modern photonics¹. Nonlinear optical processes such as second-harmonic generation (SHG) offer viable pathways toward chip-scale sources, with applications spanning sensing,³ frequency combs,^{4,5} nonlinear electro-optic modulators,^{6,7} all-optical communications,^{8,9} and quantum optics.^{10,11} Enhancing these processes necessitates maximizing both energy density¹² and spatial mode overlap¹³, thereby driving innovations in nanophotonic cavity design.

In high-Q resonant cavities, SHG conversion efficiency scales with Q^2/V , where Q is the cavity quality factor and V is the modal volume.^{14,15} Photonic crystal (PhC) nanocavities are

particularly effective at confining light in small mode volumes while maintaining high Q factors,¹⁵ making them ideal for amplifying nonlinear effects and enabling integration with resonators and waveguides.¹⁶⁻¹⁸ Theoretical studies predict substantial efficiency improvements in doubly resonant cavities by simultaneously confining both fundamental and second-harmonic modes.¹⁹⁻²¹ However, practical implementation confronts three fundamental challenges: i) out-of-plane mode leakage at SH wavelengths due to light cone limitations, ii) spatial mode mismatch between fundamental (FH) and second-harmonic (SH) modes, and iii) thermal instability under high-power operation. These issues have hindered the development of reliable on-chip light sources.

Recent advances in single-resonant silicon-carbide nanocavities with ultrahigh Q-factor have circumvented dual-resonance complexities, enabling direct SHG through precise control of coherence lengths and modal volumes.²²⁻²⁵ Building on these progresses, we demonstrate a high-Q single-resonant photonic crystal nanobeam cavity (PCNBC) on a polymer-loaded lithium niobate on insulator (LNOI) platform. By optimizing lateral confinement and longitudinal refractive index modulation, our design achieves a visible-wavelength single-lobe SH emission at 768.77 nm with a normalized conversion efficiency of 163%/W, which is more than three orders of magnitude greater than previously reported LN-based photonic crystal cavities.^{26,27} Direct CCD imaging of high-order cavity modes confirms strong spatial overlap between FH and SH modes. Furthermore, the device exhibits thermal stability under variations up to 20 °C, overcoming the thermal drift limitations of multi-resonant systems. This work provides a scalable architecture for efficient nonlinear light generation, with applications in quantum optics and chip-scale interconnects.

■ Result and Discussion

The cavity structure employed in this study, as described in Ref.²⁸, was fabricated by patterning a 400-nm-thick polymer layer on a y-cut LNOI substrate (NanoLN Inc.), comprising a 300-nm-thick LN layer and a 2- μ m-thick buried oxide (SiO₂) layer. To achieve high-efficiency SHG on this platform, a TE-polarized PCNBC design and x-axis orientation of optical path were carefully selected. These conditions ensure that the dominant optical field of the TE mode is tightly confined within the LN layer, allowing the largest nonlinear component, d_{33} , to fully contribute to the nonlinear conversion. Building upon these principles, we designed and fabricated the devices with optimized lattice parameters. Key advancements over prior PCNBC designs include a reduced lattice constant of 432 nm for visible-band SHG and 140 polymer stripes in both taper and mirror regions to balance optical transmission and quality factor. Figure 1a shows scanning electron microscopy (SEM) images of the device, featuring grating couplers for input/output coupling.

Figure 1b illustrates the dual-band (telecom/visible) experimental setup. A tunable semiconductor laser (TSL, Santec/TSL550) with manual fiber polarization control (FPC) delivered TE-polarized pump light to the cavity. Transmitted telecom light was monitored using an InGaAs photodetector (IR PD, Thorlabs/S122C) and power meter (PM, Thorlabs/PM100). The insertion loss of grating couplers is estimated to be 10.5 dB/facet. The second-harmonic (SH) emission was collected via a 200- μ m-core multimode fiber, which accommodates the mode profiles of the fundamental, second-order, and third-order modes. A 7° fiber tilt minimized reflection loss, while a spectrometer (Princeton Instruments/Acton Series SP-2500) and silicon photodetector (Thorlabs/S150C) analyzed SH spectra and power. Temperature stabilization was achieved using a thermoelectric cooler (TEC) with PID-controlled feedback from an embedded sensor.

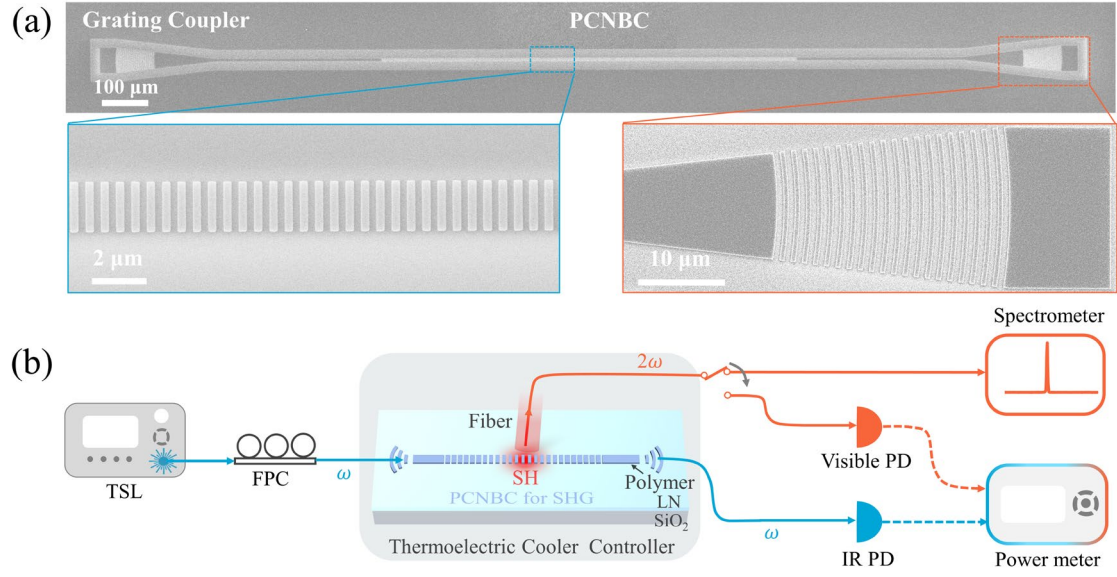


Figure 1. (a) SEM images of the fabricated PCNBC with grating couplers. (b) SHG characterization setup.

TSL: tunable semiconductor laser; FPC: fiber polarization controller; PD: photodetector.

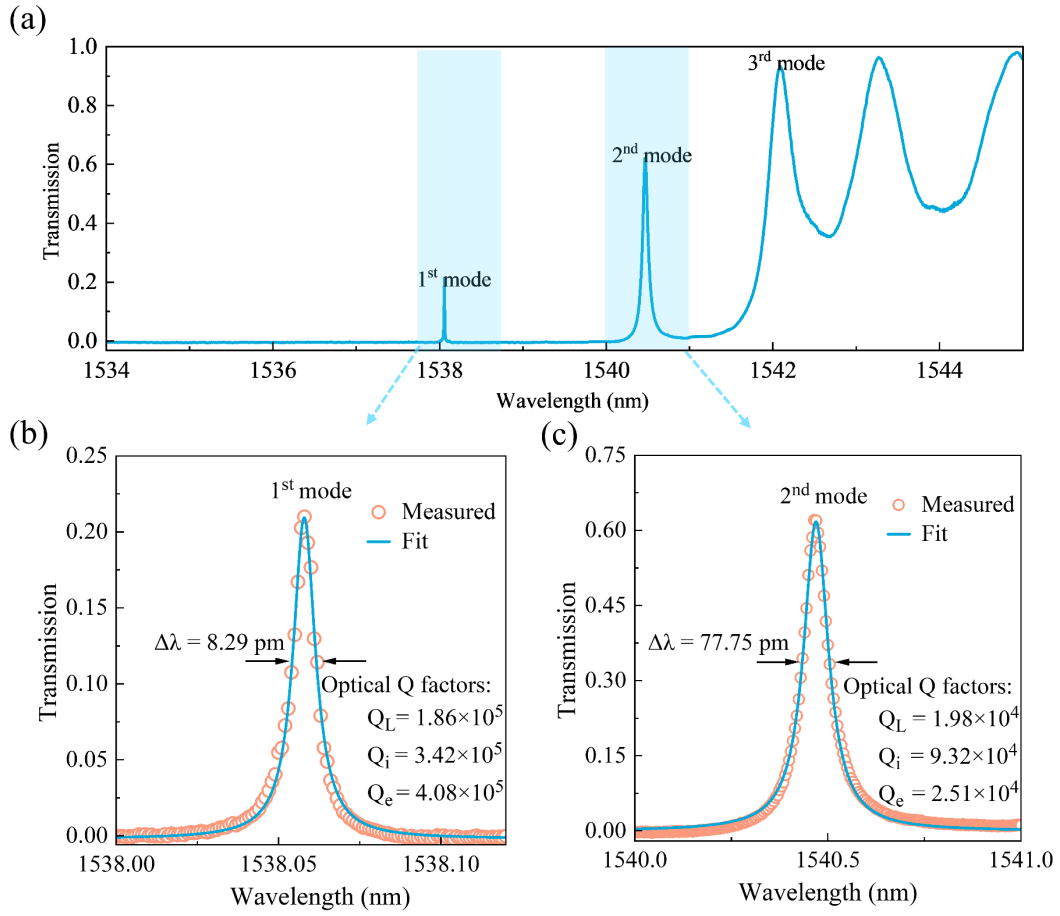


Figure 2. (a) Measured optical transmission spectrum of the PCNBC across a broad telecom band range.

(b), (c) Detailed transmission spectra of the fundamental mode (b) and the second-order mode (c) show a

loaded Q factor of 1.86×10^5 around 1538.06 nm and 1.98×10^4 around 1540.47 nm, obtained via Lorentzian fit. The extracted intrinsic Q factor (Q_i) and external coupling Q factor (Q_e) for the fundamental mode are 3.42×10^5 and 4.08×10^5 , respectively, while for the second-order mode, they are 9.32×10^4 and 2.51×10^4 .

As presented in Figure 2a, we first characterized the optical properties of the PCNBC in the telecom band by scanning the TSL wavelength from 1534.00 nm to 1545.00 nm. Resonances include fundamental mode at 1538.06 nm, second-order mode at 1540.47 nm, third-order mode at 1542.09 nm with spectra widening for higher modes due to increased losses. Figure 2b present the detailed transmission spectrum of the fundamental mode with a loaded Q factor (Q_L) of 1.86×10^5 and a high transmission of 21%. Figure 2c present the transmission spectrum of the second-order mode with a higher transmission of 62% but a lower Q_L of 1.98×10^4 . These performance metrics are better than the most PCNBCs reported to date.²⁹⁻³¹

Under high-power excitation at the fundamental mode resonance, a distinct single-lobe emission pattern was observed at the nanocavity center. CCD imaging under dark-field conditions confirmed spatial confinement consistent with simulated mode profiles. Pumping higher-order modes generated multi-lobe patterns, marking the first observation of mode-dependent SH emission profiles in PCNBCs.^{28,32} To confirm that the visible emissions correspond to SH generation, we fixed the laser wavelength at PCNBC resonances where visible emission were brightest. As shown Figure 3b, spectrometer measurements revealed SH peaks at 768.77 nm, 769.95 nm, and 770.84 nm, closely matching half the resonant wavelengths of the fundamental, second-order, and third-order modes. Minor deviations are attributed to the resolution limits of the spectrometer.

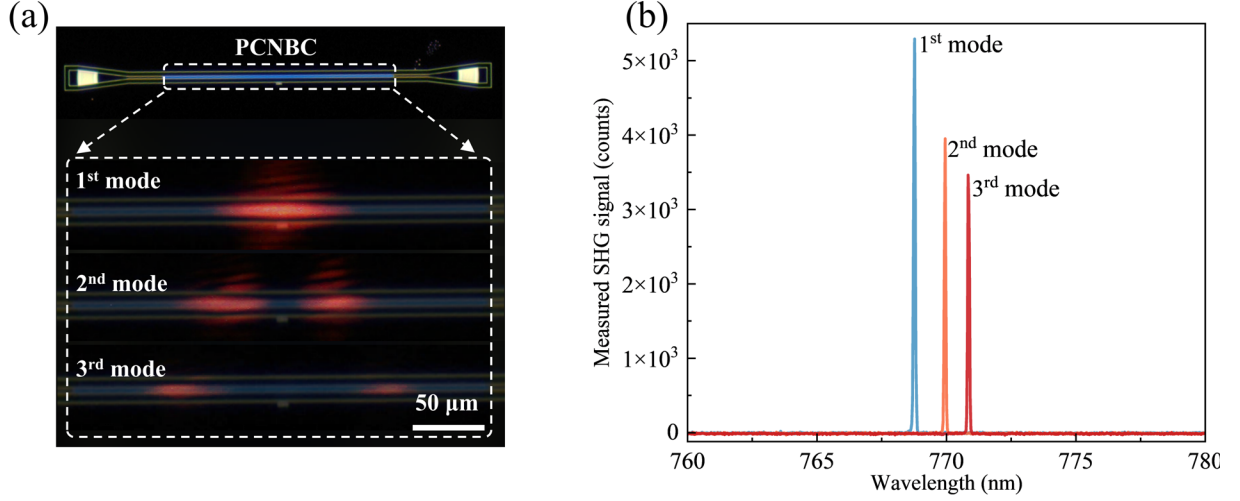


Figure 3. (a) SH emission patterns for fundamental, second-order, and third-order modes, respectively. (b) SH spectra recorded at fixed laser wavelengths for each resonant mode.

Using classical temporal coupled-mode theory,³³ we estimate the intracavity pump power (P_{cav}) contributing to SHG conversion. In the nondepleted (low pump power) regime, the intracavity field of the resonance mode is unaffected by the SHG process. Thus, in steady state, P_{cav} can be expressed as

$$P_{\text{cav}} = \eta_{\text{cav}} P_{\text{in}} = \frac{2\tau_{\text{t}}^2}{\tau_{\text{i}}\tau_{\text{e}}} P_{\text{in}} \quad (1)$$

where τ_{t} , τ_{i} and τ_{e} represent the total, intrinsic, and external lifetimes of the resonance mode ($\tau_{\text{t}}^{-1} = \tau_{\text{i}}^{-1} + \tau_{\text{e}}^{-1}$). P_{in} is the pump power after the grating coupler. Combining transmission spectra with the extracted Q factors in Figure 2, we calculate η_{cav} for each resonance mode.

The normalized SHG conversion efficiency η can be defined as $\eta = \frac{P_{\text{SHG}}}{P_{\text{cav}}^2}$.

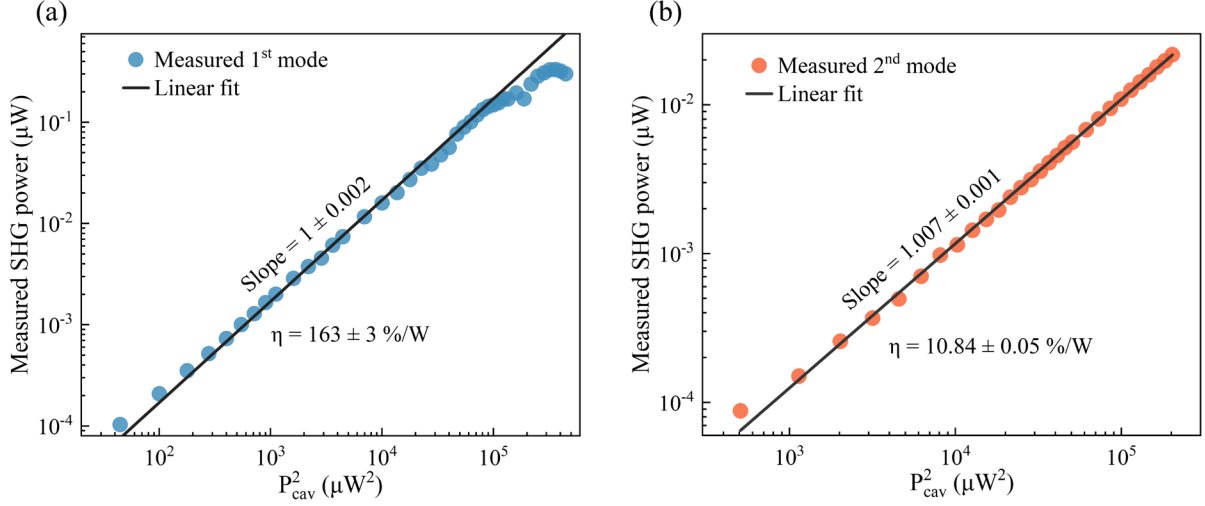


Figure 4. (a), (b) SHG power (P_{SHG}) versus the squared intracavity pump power (P_{cav}^2) for the fundamental mode (a) and the second-order mode (b). The solid line represents a linear fit in the nondepleted region, with a normalized SHG conversion efficiency of 163%/W for the fundamental mode and 10.84%/W for the second-order mode.

Figure 4a shows the SHG power P_{SHG} versus P_{cav}^2 for the fundamental mode. In the non-pump depleted regime ($P_{\text{cav}} < 400 \mu\text{W}$), the linear fit (slope=1) confirms the expected quadratic dependence, yielding a normalized conversion efficiency of 163%/W with an uncertainty of 3%/W. At higher powers ($P_{\text{cav}} > 400 \mu\text{W}$), deviations from quadratic scaling indicate pump depletion, with the absolute efficiency reaching 0.055% at P_{cav} of 601.72 μW . For the second-order mode, the normalized efficiency drops to 10.84%/W due to its lower Q factor.²⁴

Table 1 benchmarks SHG efficiencies across photonic crystal cavities platforms. While SiC cavities achieve higher efficiencies, their SHG emission patterns deviate spatially from the FH modes, which would introduce challenges in subsequent processes such as light source collimation, fiber transmission, and inter-chip coupling.³⁴⁻³⁶ In contrast, our LN-based PCNBC achieves a normalized efficiency of 163%/W, which is more than three orders of magnitude higher than the other LN PhC cavities. In addition to its high SHG conversion efficiency, an important feature of our device is that the generated SH emission perfectly matches the

fundamental harmonic modes, making it particularly suitable as a light source for photonic integrated circuits (PICs).

Table 1 Comparison of SHG conversion efficiencies for photonic crystal cavities

Cavity type/Platform	$Q_L (\times 10^4)$	SH collection method	η (%/W)	SH mode consistent with FH mode
2D PhC/SiC ²³	60	Microscope objective	1900	No
2D PhC/SiC ²⁴	71	Microscope objective	4000	No
2D PhC/GaP ³⁷	0.56	Microscope objective	430	No
2D PhC/GaAs ³⁸	0.4	Microscope objective	1.2	No
2D PhC/LN ²⁷	0.05	Microscope objective	1.2×10^{-2}	No
2D PhC/LN ²⁶	33.4	Tapered optical fiber	7.8×10^{-2}	Yes
PCNBC/LN ³⁹	5.4	Tapered optical fiber	0.4×10^{-3}	Yes
PCNBC/LN ^{This work}	18.6	Multimode fiber	163	Yes

As illustrated in Figure 5a, thermal tuning tests reveal a redshift in both pump and SH wavelengths with increasing temperature, consistent with the thermo-optic effect. The SH wavelength is recorded via the spectrometer when the laser wavelength is fixed at the resonance wavelength of the fundamental mode, with a low P_{cav} of 34 μW . The pump wavelength shifts with a linear fitted temperature tuning rate of 26.8 ± 0.23 pm/ $^{\circ}\text{C}$ is roughly twice that of the SH of 13.5 ± 0.37 pm/ $^{\circ}\text{C}$. Crucially, as shown in Figure 5b, SHG conversion efficiency remains stable across a 20 $^{\circ}\text{C}$ range, demonstrating robustness against thermal drift which is a key advantage over multi-resonant or phase match SHG devices.^{40,41}

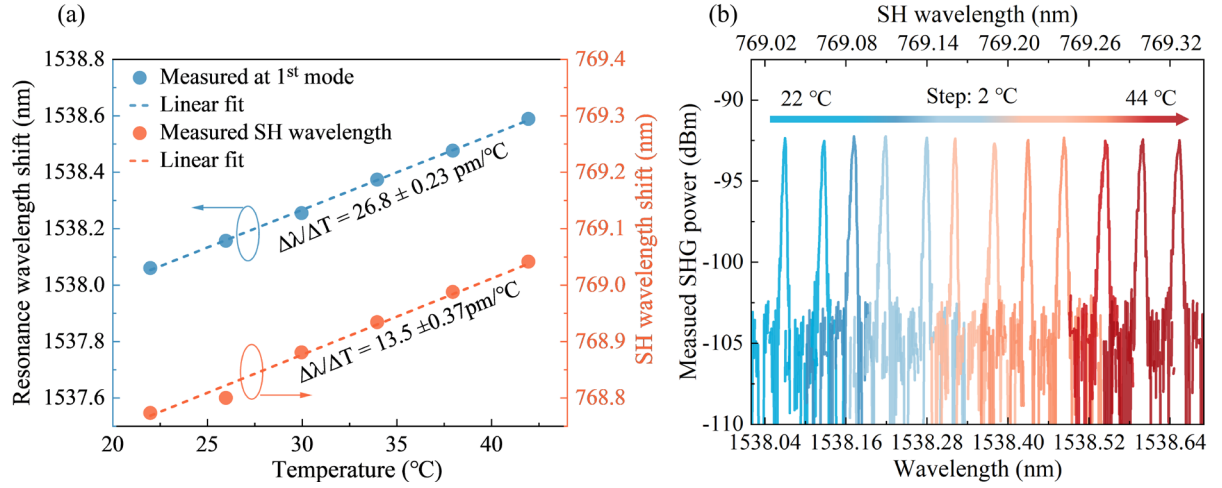


Figure 5. (a) Resonance wavelength shifts for pump (fundamental mode) and SH light versus temperature. (b) SH spectra show consistent peak power at different temperatures.

■ CONCLUSIONS

In conclusion, we have proposed and experimentally demonstrated a high-Q single-resonant nanocavity for efficient SHG on polymer-loaded y-cut LNOI platform. The device emits a bright single-lobe radiation pattern at 768.77 nm, achieving a normalized SHG conversion efficiency of 163%/W, which is more than three orders of magnitude higher than that of previous similar microcavities. In addition, the devices exhibit exceptional temperature stability, with no significant significant efficiency degradation over a 20 °C range. Importantly, this approach is not limited to the LN material, but may also be universally applied to other photonics platforms, such as barium titanate (BTO), aluminum nitrogen (AlN), particularly for materials that are difficult to be etched. Our work establishes a scalable architecture for ultracompact nonlinear light sources, with applications in quantum optics and chip-scale interconnects.

AUTHOR INFORMATION

Corresponding Authors

Danyang Yao – State Key Laboratory of Wide-Bandgap Semiconductor Devices and Integrated Technology, School of Microelectronics, Faculty of integrated circuits, Xidian University, Xi'an 710071, China; Email: dyyao@xidian.edu.cn;

Xuetao Gan – Key Laboratory of Light Field Manipulation and Information Acquisition, Ministry of Industry and Information Technology, and Shaanxi Key Laboratory of Optical Information Technology, School of Physical Science and Technology, Northwestern Polytechnical University, Xi'an, 710129, China; Email: xuetaogan@nwpu.edu.cn;

Jinchuan Zhang – Laboratory of Solid-State Optoelectronics Information Technology, Institute of Semiconductors, Chinese Academy of Sciences, Beijing 100083, China; Email: zhangjinchuan@semi.ac.cn;

Authors

Zhi Jiang – State Key Laboratory of Wide-Bandgap Semiconductor Devices and Integrated Technology, School of Microelectronics, Faculty of integrated circuits, Xidian University, Xi'an 710071, China

Yu Gao – State Key Laboratory of Wide-Bandgap Semiconductor Devices and Integrated Technology, School of Microelectronics, Faculty of integrated circuits, Xidian University, Xi'an 710071, China

Xu Ran – State Key Laboratory of Wide-Bandgap Semiconductor Devices and Integrated Technology, School of Microelectronics, Faculty of integrated circuits, Xidian University, Xi'an 710071, China

Duomao Li – State Key Laboratory of Wide-Bandgap Semiconductor Devices and Integrated Technology, School of Microelectronics, Faculty of integrated circuits, Xidian University, Xi'an 710071, China

Erqi Zhang – State Key Laboratory of Wide-Bandgap Semiconductor Devices and Integrated Technology, School of Microelectronics, Faculty of integrated circuits, Xidian University, Xi'an 710071, China

Jianguo Wang – Key Laboratory of Light Field Manipulation and Information Acquisition, Ministry of Industry and Information Technology, and Shaanxi Key Laboratory of Optical Information Technology, School of Physical Science and Technology, Northwestern Polytechnical University, Xi'an, 710129, China

Fengqi Liu - Laboratory of Solid-State Optoelectronics Information Technology, Institute of Semiconductors, Chinese Academy of Sciences, Beijing 100083, China

Yue Hao – State Key Laboratory of Wide-Bandgap Semiconductor Devices and Integrated Technology, School of Microelectronics, Faculty of integrated circuits, Xidian University, Xi'an 710071, China

Notes

The authors declare no competing financial interest.

ACKNOWLEDGMENT

This work was supported by the Chinese Institute of Electronics-Smartchip Special Research Program, the National Natural Science Foundation of China (Grant No. 62293522 and 62235016), and the Fundamental Research Funds for the Central Universities.

REFERENCES

- (1) Zhang, X.; Zhou, Z.; Guo, Y.; Zhuang, M.; Jin, W.; Shen, B.; Chen, Y.; Huang, J.; Tao, Z.; Jin, M.; et al. High-coherence parallelization in integrated photonics. *Nat. Communications* **2024**, 15 (1), 7892.
- (2) Luo, R.; Jiang, H.; Rogers, S.; Liang, H.; He, Y.; Lin, Q. On-chip second-harmonic generation and broadband parametric down-conversion in a lithium niobate microresonator.

Opt. Express **2017**, 25 (20), 24531-24539.

- (3) Ngo, G. Q.; Najafidehaghani, E.; Gan, Z.; Khazaei, S.; Siems, M. P.; George, A.; Schartner, E. P.; Nolte, S.; Ebendorff-Heidepriem, H.; Pertsch, T.; et al. In-fibre second-harmonic generation with embedded two-dimensional materials. *Nat. Photonics* **2022**, 16 (11), 769-776.
- (4) Ricciardi, I.; Maddaloni, P.; De Natale, P.; Erkintalo, M.; Hansson, T.; Arie, A.; Wabnitz, S.; De Rosa, M. Optical frequency combs in dispersion-controlled doubly resonant second-harmonic generation. *Opt. Express* **2022**, 30 (25), 45694-45704.
- (5) Szabados, J.; Puzyrev, D. N.; Minet, Y.; Reis, L.; Buse, K.; Villois, A.; Skryabin, D. V.; Breunig, I. Frequency Comb Generation via Cascaded Second-Order Nonlinearities in Microresonators. *Phys. Rev. Lett.* **2020**, 124 (20), 203902.
- (6) Wang, J.; Han, N.; Luo, Z. D.; Zhang, M.; Chen, X.; Liu, Y.; Hao, Y.; Zhao, J.; Gan, X. Electrically Tunable Second Harmonic Generation in Atomically Thin ReS₂. *ACS Nano* **2022**, 16 (4), 6404-6413.
- (7) Seyler, K. L.; Schaibley, J. R.; Gong, P.; Rivera, P.; Jones, A. M.; Wu, S.; Yan, J.; Mandrus, D. G.; Yao, W.; Xu, X. Electrical control of second-harmonic generation in a WSe₂ monolayer transistor. *Nat. Nanotechnol* **2015**, 10 (5), 407-411.
- (8) Ishizuki, H.; Suhara, T.; Fujimura, M.; Nishihara, H. Wavelength conversion type picosecond optical switching by waveguide QPM SHG/DFG device. *Opt. Quantum Electron.* **2001**, 33, 953-961.
- (9) Fryett, T. K.; Dodson, C. M.; Majumdar, A. Cavity enhanced nonlinear optics for few photon optical bistability. *Opt. Express* **2015**, 23 (12), 16246-16255.
- (10) Tanzilli, S.; Tittel, W.; Halder, M.; Alibart, O.; Baldi, P.; Gisin, N.; Zbinden, H. A photonic quantum information interface. *Nature* **2005**, 437 (7055), 116-120.
- (11) Lu, J.; Li, M.; Zou, C.-L.; Al Sayem, A.; Tang, H. X. Toward 1% single-photon anharmonicity with periodically poled lithium niobate microring resonators. *Optica* **2020**, 7

(12), 1654-1659.

(12) Rarick, H.; Kala, A.; Pumulo, S.; Manna, A.; Sharp, D.; Munley, C.; Xu, X.; Majumdar, A. Enhanced Second-Harmonic Generation in a Monolayer Tungsten Diselenide Integrated Silicon Nitride Nanocavity. *Acs Photonics* **2024**, 11 (11), 4635-4641.

(13) Smith, R. Theory of intracavity optical second-harmonic generation. *IEEE J. Quantum Electron.* **1970**, 6 (4), 215-223.

(14) Rodriguez, A.; Soljačić, M.; Joannopoulos, J. D.; Johnson, S. G. $\chi^{(2)}$ and $\chi^{(3)}$ harmonic generation at a critical power in inhomogeneous doubly resonant cavities. *Opt. Express* **2007**, 15 (12), 7303-7318.

(15) Deotare, P. B.; McCutcheon, M. W.; Frank, I. W.; Khan, M.; Lončar, M. High quality factor photonic crystal nanobeam cavities. *Appl. Phys. Lett.* **2009**, 94 (12), 121106.

(16) Galli, M.; Gerace, D.; Welna, K.; Krauss, T. F.; O’Faolain, L.; Guizzetti, G.; Andreani, L. C. Low-power continuous-wave generation of visible harmonics in silicon photonic crystal nanocavities. *Opt. Express* **2010**, 18 (25), 26613-26624.

(17) Rivoire, K.; Buckley, S.; Hatami, F.; Vučković, J. Second harmonic generation in GaP photonic crystal waveguides. *Appl. Phys. Lett.* **2011**, 98 (26), 263113.

(18) Yao, D.; Jiang, Z.; Zhang, Y.; Xie, H.; Wang, T.; Wang, J.; Gan, X.; Han, G.; Liu, Y.; Hao, Y. Ultrahigh thermal-efficient all-optical silicon photonic crystal nanobeam cavity modulator with TPA-induced thermo-optic effect. *Opt. Lett.* **2023**, 48 (9), 2325-2328.

(19) Liscidini, M.; Andreani, L. C. Highly efficient second-harmonic generation in doubly resonant planar microcavities. *Appl. Phys. Lett.* **2004**, 85 (11), 1883-1885.

(20) Liscidini, M.; Claudio Andreani, L. Second-harmonic generation in doubly resonant microcavities with periodic dielectric mirrors. *Phys. Rev. E* **2006**, 73 (1), 016613.

(21) Paschotta, R.; Fiedler, K.; Kürz, P.; Mlynek, J. Nonlinear mode coupling in doubly resonant frequency doublers. *Appl. Phys. B-Lasers Opt.* **1994**, 58 (2), 117-122.

- (22) Yamada, S.; Song, B.-S.; Jeon, S.; Upham, J.; Tanaka, Y.; Asano, T.; Noda, S. Second-harmonic generation in a silicon-carbide-based photonic crystal nanocavity. *Opt. Lett.* **2014**, 39 (7), 1768-1771.
- (23) Song, B.-S.; Asano, T.; Jeon, S.; Kim, H.; Chen, C.; Kang, D. D.; Noda, S. Ultrahigh-Q photonic crystal nanocavities based on 4H silicon carbide. *Optica* **2019**, 6 (8), 991-995.
- (24) Kim, H.; Noda, S.; Song, B.-S.; Asano, T. Determination of Nonlinear Optical Efficiencies of Ultrahigh-Q Photonic Crystal Nanocavities with Structural Imperfections. *Acs Photonics* **2021**, 8 (10), 2839-2845.
- (25) Kim, H.; Song, B.-S.; Asano, T.; Noda, S. Enhanced second-harmonic generation in a photonic crystal waveguide-coupled nanocavity using a wavelength-selective reflector. *Appl Photonics* **2023**, 8 (12), 121303.
- (26) Li, M.; Liang, H.; Luo, R.; He, Y.; Lin, Q. High-Q 2D Lithium Niobate Photonic Crystal Slab Nanoresonators. *Laser Photon. Rev.* **2019**, 13 (5), 1800228.
- (27) Diziain, S.; Geiss, R.; Zilk, M.; Schrepel, F.; Kley, E. B.; Tünnermann, A.; Pertsch, T. Second harmonic generation in free-standing lithium niobate photonic crystal L3 cavity. *Appl. Phys. Lett.* **2013**, 103 (5), 051117.
- (28) Jiang, Z.; Fang, C.; Ran, X.; Gao, Y.; Wang, R.; Wang, J.; Yao, D.; Gan, X.; Liu, Y.; Hao, Y.; et al. Ultra-high-Q photonic crystal nanobeam cavity for etchless lithium niobate on insulator (LNOI) platform. *Opto-Electron. Adv.* **2025**, 8 (1), 240114.
- (29) Zhang, J.; Pan, B.; Liu, W.; Dai, D.; Shi, Y. Ultra-compact electro-optic modulator based on etchless lithium niobate photonic crystal nanobeam cavity. *Opt. Express* **2022**, 30 (12), 20839-20846.
- (30) Li, M.; Ling, J.; He, Y.; Javid, U. A.; Xue, S.; Lin, Q. Lithium niobate photonic-crystal electro-optic modulator. *Nat. Commun* **2020**, 11 (1), 4123.
- (31) Witmer, J. D.; Valery, J. A.; Arrangoiz-Arriola, P.; Sarabalis, C. J.; Hill, J. T.; Safavi-Naeini,

A. H. High-Q photonic resonators and electro-optic coupling using silicon-on-lithium-niobate. *Sci Rep* **2017**, 7 (1), 46313.

(32) von Keitz, J.; Feldmann, J.; Gruhler, N.; Ríos, C.; Wright, C. D.; Bhaskaran, H.; Pernice, W. H. P. Reconfigurable Nanophotonic Cavities with Nonvolatile Response. *Acs Photonics* **2018**, 5 (11), 4644-4649.

(33) Meade, R. D. V. E.; Johnson, S. G.; Winn, J. N. *Photonic Crystals: Molding the Flow of Light*, Second Edition; Princeton University Press, 2008.

(34) Westover, T.; Olsen, S.; Westhoff, Z.; Morrill, N.; Davis, R.; Vanfleet, R. Visible and short-wavelength infrared light collimation through carbon nanotube, parallel-hole collimators. *Opt. Express* **2022**, 30 (13), 22679-22686.

(35) Kaushik, P.; Singh, D. P.; Rajpoot, S. Fibre Optic Communication In 21st Century. In *2020 International Conference on Intelligent Engineering and Management (ICIEM)*; IEE: London, UK, 2020; pp 125-129.

(36) Davanco, M.; Liu, J.; Sapienza, L.; Zhang, C.-Z.; De Miranda Cardoso, J. V.; Verma, V.; Mirin, R.; Nam, S. W.; Liu, L.; Srinivasan, K. Heterogeneous integration for on-chip quantum photonic circuits with single quantum dot devices. *Nat. Commun.* **2017**, 8 (1), 889.

(37) Rivoire, K.; Lin, Z.; Hatami, F.; Masselink, W. T.; Vuckovic, J. Second harmonic generation in gallium phosphide photonic crystal nanocavities with ultralow continuous wave pump power. *Opt. Express* **2009**, 17 (25), 22609-22615.

(38) Buckley, S.; Radulaski, M.; Petykiewicz, J.; Lagoudakis, K. G.; Kang, J.-H.; Brongersma, M.; Biermann, K.; Vučković, J. Second-Harmonic Generation in GaAs Photonic Crystal Cavities in (111)B and (001) Crystal Orientations. *Acs Photonics* **2014**, 1 (6), 516-523.

(39) Jiang, H.; Liang, H.; Luo, R.; Chen, X.; Chen, Y.; Lin, Q. Nonlinear frequency conversion in one dimensional lithium niobate photonic crystal nanocavities. *Appl. Phys. Lett.* **2018**, 113 (2), 021104.

- (40) Wu, X.; Hao, Z.; Zhang, L.; Jia, D.; Ma, R.; Tao, C.; Gao, F.; Bo, F.; Zhang, G.; Xu, J. Second-Harmonic Generation with a $440000\%W^{-1}$ Conversion Efficiency in a Lithium Niobate Microcavity without Periodic Poling. *Laser Photon. Rev.* **2024**, 18 (7), 2300951.
- (41) Bruch, A. W.; Liu, X.; Guo, X.; Surya, J. B.; Gong, Z.; Zhang, L.; Wang, J.; Yan, J.; Tang, H. X. 17 000%/W second-harmonic conversion efficiency in single-crystalline aluminum nitride microresonators. *Appl. Phys. Lett.* **2018**, 113 (13), 131102.